

Boosting Quantitive and Spatial Awareness for Zero-Shot Object Counting

Da Zhang^{1,2*} Bingyu Li^{2,3} Feiyu Wang^{2,4} Zhiyuan Zhao² Junyu Gao^{1,2†}

¹Northwestern Polytechnical University ²Institute of Artificial Intelligence (TeleAI), China Telecom

³University of Science and Technology of China ⁴Fudan University

{dazhang900, tuzixini, gjy3035}@gmail.com,

libingyu0205@mail.ustc.edu.cn, wangfy25@m.fudan.edu.cn

Abstract

Zero-shot object counting (ZSOC) aims to enumerate objects of arbitrary categories specified by text descriptions without requiring visual exemplars. However, existing methods often treat counting as a coarse retrieval task, suffering from a lack of fine-grained quantity awareness. Furthermore, they frequently exhibit spatial insensitivity and degraded generalization due to feature space distortion during model adaptation. To address these challenges, we present **QICA**, a novel framework that synergizes quantity perception with robust spatial cast aggregation. Specifically, we introduce a Synergistic Prompting Strategy (SPS) that adapts vision and language encoders through numerically conditioned prompts, bridging the gap between semantic recognition and quantitative reasoning. To mitigate feature distortion, we propose a Cost Aggregation Decoder (CAD) that operates directly on vision-text similarity maps. By refining these maps through spatial aggregation, CAD prevents overfitting while preserving zero-shot transferability. Additionally, a multi-level quantity alignment loss (\mathcal{L}_{MQA}) is employed to enforce numerical consistency across the entire pipeline. Extensive experiments on FSC-147 demonstrate competitive performance, while zero-shot evaluation on CARPK and ShanghaiTech-A validates superior generalization to unseen domains. Code will be [available](#).

1. Introduction

Object counting is a fundamental computer vision task with wide ranging applications including urban surveillance [38], ecological monitoring [45, 68], and inventory management [3]. Traditional methods often focused on specific object categories requiring extensive annotated datasets for each class, limiting their scalability and adaptability to unseen scenarios [13, 16, 33, 58]. To address this inflexibility, recent

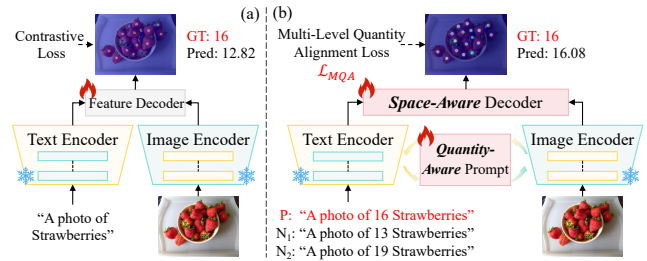


Figure 1. A comparison between (a) standard ZSOC and (b) QICA. (a) Existing methods typically rely on unimodal prompting and direct feature interaction, suffering from a lack of **fine-grained quantity awareness** and **spatial insensitivity**, which often leads to overfitting. (b) QICA introduces numerically conditional collaborative prompts and achieves accurate density estimation through cost aggregation decoding via \mathcal{L}_{MQA} .

research has explored class agnostic counting paradigms [37, 49]. Among these, zero shot object counting (ZSOC) [62] presents a highly desirable goal aiming to count objects of any category specified by natural language text descriptions without needing category specific training data or visual exemplars during inference [22, 43, 56].

The advent of large-scale vision-language models (VLMs) pretrained on massive image-text pairs has significantly advanced ZSOC capabilities [6, 28, 31, 39]. These models learn a joint embedding space that enables associating visual content with textual descriptions [2, 23, 66]. Current ZSOC methods typically employ a VLM encoder to extract image features and text embeddings, compute vision-language similarity maps to roughly locate potential object regions, and process these features through a downstream decoder for density map prediction [32, 47]. While this paradigm has shown promising results, it faces fundamental challenges stemming from the gap between image-level VLM pretraining and pixel-level density estimation requirements [59, 67].

A critical yet often overlooked limitation is the **lack of fine-grained quantity awareness** in existing text-prompted

*Work done during an internship at TeleAI.

†Corresponding author.

counting methods [44, 53]. While text prompts effectively specify target categories, they typically do not provide supervision regarding object quantities [69]. Current models are primarily trained to align visual features with categorical semantics, essentially learning what an object looks like but not what constitutes different quantities visually [64]. Text prompts usually specify only object categories without incorporating numerical context, resulting in encoders that excel at recognizing what objects are but struggle to understand how many exist [9, 17, 41]. This quantity blindness hinders the ability to accurately distinguish between scenes containing varying numbers of objects, limiting precision especially in dense scenarios where understanding numerical differences is crucial [14, 46].

Another challenge arises during adaptation of pretrained VLMs to counting tasks [15, 48, 51]. Directly fine-tuning VLM encoders within conventional feature aggregation frameworks often leads to severe overfitting on training categories [12, 24, 29, 71]. This fine-tuning process can distort the pretrained feature space, critically impairing generalization to unseen object classes during zero-shot inference. Existing adaptation strategies that operate on intermediate feature representations risk projecting embeddings into task-specific spaces that deviate from the original pretrained manifold [60]. Furthermore, present architectures often exhibit **spatial insensitivity** due to coarse aggregation mechanisms that neglect fine-grained details. Together with feature space distortion, this forces a compromise: current ZSOC approaches often resort to freezing VLM encoders entirely, sacrificing the potential benefits of adapting powerful representations to counting-specific requirements [30, 36, 40].

To overcome these limitations, we introduce QICA, a novel framework for ZSOC based on quantity-aware synergistic prompting and cost spatial aggregation (as shown in Figure 1). To instill quantity awareness, we propose a **synergistic prompting strategy (SPS)** that conditions learnable prompts in both text and vision encoders on numerical information. Unlike conventional approaches that treat branches independently, our prompts are linked via a coupling function enabling bidirectional gradient flow and joint adaptation toward quantity understanding. During training, we dynamically generate quantity-oriented text prompts with factual and counterfactual numerical values to teach fine-grained quantity distinction. To address the fine-tuning challenge, we introduce a **cost aggregation decoder (CAD)** that operates directly on vision-text similarity maps. By refining similarity maps through robust spatial aggregation, our approach mitigates overfitting while preserving generalization to unseen classes. Furthermore, we propose a **multi-level quantity alignment loss (\mathcal{L}_{MQA})** that enforces numerical consistency across encoder and decoder stages through ranking constraints on embeddings and auxiliary losses.

Extensive experiments demonstrate the effectiveness of

our approach. QICA achieves competitive performance on FSC-147, significantly outperforming existing text-prompted counting methods. Cross-dataset evaluation on CARPK and ShanghaiTech-A further validates strong generalization capability to unseen domains without any fine-tuning. In summary, we make the following contributions:

- We propose the SPS to instill fine-grained quantity awareness. By leveraging explicit numerical conditioning and bidirectional gradient coupling, it achieves effective joint adaptation of vision and language encoders.
- To address spatial insensitivity and prevent feature space distortion, we introduce the CAD. It operates directly on similarity maps to preserve spatial structure while enabling robust fine-tuning.
- We introduce \mathcal{L}_{MQA} that enforces strict numerical consistency across both encoder and decoder stages through ranking constraints and auxiliary supervision.
- Experiments on FSC-147 and cross-dataset validation confirm the effectiveness of QICA.

2. Related Work

2.1. Class-Agnostic Object Counting

Early object counting research focused on category-specific scenarios where models were trained to count particular object types such as crowds [35, 38, 54, 58], vehicles [4, 7, 20], or cells [18, 61]. These specialized approaches achieved strong performance within their target domains but required extensive retraining for new categories [4]. Class-agnostic counting emerged to address this limitation by formulating the task as a similarity matching problem between image regions and provided exemplars [37, 49]. Pioneering works introduced architectures that compute feature correspondences between query images and reference patches to localize and count target objects [63]. Subsequent methods enhanced this paradigm through improved feature extraction with advanced backbones, refined matching mechanisms via multi-scale feature fusion, and sophisticated similarity metric learning [11, 26, 62]. While these exemplar-based approaches demonstrate impressive generalization across diverse object categories, they inherently require manual annotation of reference patches during inference, limiting their practical applicability in dynamic scenarios [10, 32, 34, 37, 50, 52]. Our QICA framework eliminates this dependency by leveraging text descriptions rather than visual exemplars for category specification.

2.2. Text-Prompted Zero-Shot Counting

The advent of large-scale VLMs has enabled zero-shot object counting through natural language specification [31, 48]. Early approaches in this direction employed text-conditioned generative models to synthesize visual exemplars from text descriptions, which were then used in conventional exemplar-

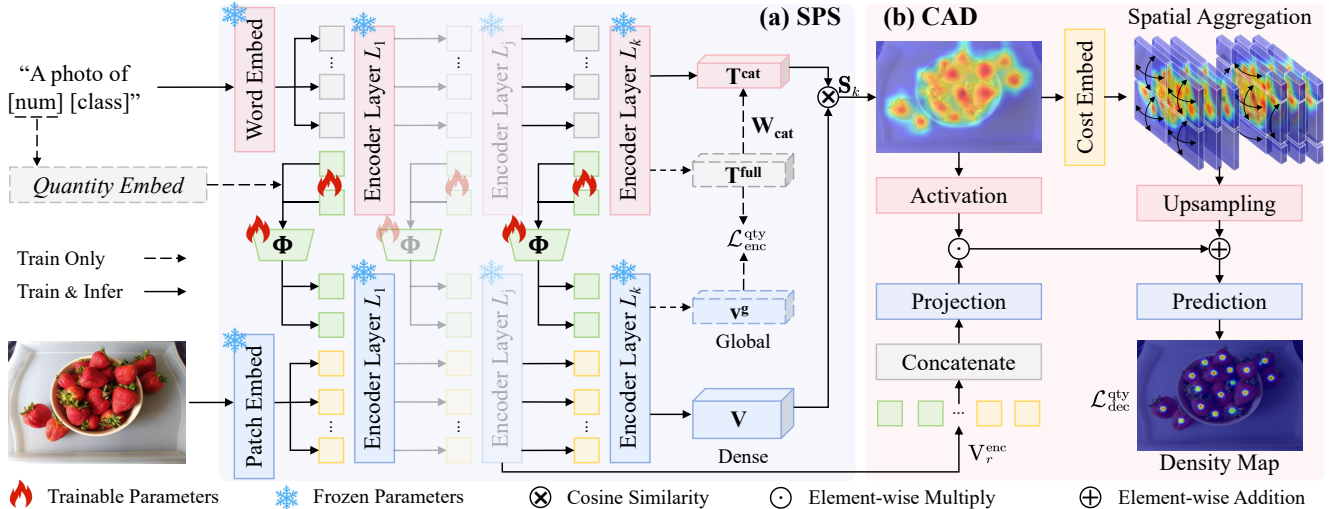


Figure 2. **Overall architecture of QICA.** (a) **SPS** jointly adapts the frozen vision and language encoders by mapping quantity-aware text prompts to visual prompts via a coupling function (Φ). (b) **CAD** first computes a similarity map between dense visual features (V) and category-only text embeddings (T^{cat}), then refines this map through spatial aggregation and multi-scale upsampling to predict the final density map. The entire framework is supervised by \mathcal{L}_{MQA} . Notably, the pathways involving explicit quantity information (Quantity Embed and T^{full}) are active only during training, while the model uses only category information at inference to ensure zero-shot generalization.

based counting frameworks [8, 57, 72]. More recent methods directly leverage pretrained vision-language models to extract joint image-text representations [25]. These approaches typically compute similarity between dense image features and text embeddings to generate localization maps, which are subsequently processed by CNN-based decoders for density prediction [28]. Various techniques have been proposed to enhance this paradigm, including hierarchical feature interaction modules, semantic-conditioned prompt tuning for visual encoders, and multi-stage architectures combining region proposal networks with vision-language matching [2, 47, 69]. However, these methods predominantly focus on categorical alignment while treating quantity information implicitly. Recent work has begun exploring numerical information in text prompts but applies uniform treatment to different quantity values without capturing fine-grained numerical relationships [9, 17, 41]. Furthermore, most existing approaches freeze vision-language encoders to avoid overfitting, sacrificing adaptation potential [36, 43]. In contrast, QICA introduces quantity-conditioned prompting with explicit numerical supervision through ranking constraints and employs cost aggregation on similarity maps to enable robust encoder fine-tuning without compromising generalization.

3. Methodology

3.1. Problem Formulation

Given an input image $I \in \mathbb{R}^{H \times W \times 3}$ and a text description T specifying the target object category, our goal is to predict a density map $D \in \mathbb{R}^{H \times W}$ where the integral of D corresponds to the total count of specified objects. During training,

we have access to a dataset $\mathcal{D}_{\text{train}} = \{(I_i, T_i, D_i^{\text{GT}})\}_{i=1}^N$ containing images with corresponding text prompts and ground truth density maps. At inference time, the model receives novel images with text descriptions of potentially unseen categories and must predict accurate density maps without access to visual exemplars or category-specific training. The proposed QICA architecture is shown in Figure 2.

3.2. Synergistic Prompting Strategy

SPS adapts both vision and language encoders of a pretrained VLM through learnable tokens explicitly conditioned on numerical information. Our approach builds upon the observation that standard prompt tuning treats vision and language branches independently, limiting their joint adaptation for quantity-aware tasks [17, 29, 71].

To incorporate numerical information into the prompting process, we first transform discrete quantity values into continuous representations. Given a quantity value q , we obtain its embedding through an embedding layer followed by linear projection, yielding $\epsilon_q \in \mathbb{R}^{d_t}$ where d_t denotes the text encoder dimension. During training, we generate multiple quantity values including the ground truth count n^{gt} and counterfactual values $\{n^{\text{gt}} \pm k\delta\}$ where δ is dynamically determined based on n^{gt} following interval-based binning strategy (see Appendix). This produces K quantity embeddings $\{\epsilon_{q_0}, \epsilon_{q_1}, \dots, \epsilon_{q_{K-1}}\}$.

For each layer j in the first L layers of the text encoder, we introduce learnable prompt tokens $\Pi^j = [\pi_1^j, \pi_2^j, \dots, \pi_m^j] \in \mathbb{R}^{m \times d_t}$ where m denotes the prompt length. To condition these prompts on quantity information,

we compute quantity-aware prompts as

$$\hat{\Pi}_k^j = \Pi^j + \epsilon_{q_k} \mathbf{1}^T \quad (1)$$

where $\mathbf{1} \in \mathbb{R}^m$ is a vector of ones and k indexes the quantity hypothesis. The outer product broadcasts the quantity embedding across all prompt positions. These conditioned prompts are prepended to word embeddings of text descriptions, forming an input sequence that is processed through the text encoder layers.

Following the principle of maintaining training-inference consistency, the text encoder produces two types of embeddings during training. The complete embedding $\mathbf{T}_k^{\text{full}}$ extracted from the final token output captures both categorical and numerical semantics from text descriptions containing numerical values. The category embedding $\mathbf{T}_k^{\text{cat}}$ is obtained by removing the influence of quantity tokens through a learned linear projection \mathbf{W}_{cat} , formally expressed as

$$\mathbf{T}_k^{\text{cat}} = \mathbf{W}_{\text{cat}}(\mathbf{T}_k^{\text{full}}) \quad (2)$$

At inference time, input text contains only category information without numerical values. To ensure training-inference consistency, we employ a dual-path strategy: during training, quantity-aware prompts generate complete embeddings \mathbf{T}^{full} , which are then projected through \mathbf{W}_{cat} to extract category-only semantics \mathbf{T}^{cat} . During inference, category-only prompts naturally produce embeddings with identical semantic content to \mathbf{T}^{cat} , bypassing the need for \mathbf{W}_{cat} projection. This design ensures that similarity computation receives semantically equivalent category embeddings in both phases, maintaining consistent decoder inputs despite different computational pathways.

To establish synergistic adaptation between modalities, we introduce coupling functions $\{\Phi^j\}_{j=1}^L$ that project language prompts to vision prompts as

$$\Psi_k^j = \Phi^j(\hat{\Pi}_k^j) \quad (3)$$

where Φ^j is implemented as a linear projection from d_t to d_v . These vision prompts are inserted into corresponding layers of the vision encoder alongside image patch embeddings. This coupling mechanism enables bidirectional gradient flow where updates to language prompts influence vision prompts and vice versa, facilitating joint adaptation of both encoders toward quantity-sensitive feature extraction. The vision encoder processes the image to produce dense visual embeddings $\mathbf{V} \in \mathbb{R}^{(h \times w) \times d_v}$ and global image representation $\mathbf{v}^g \in \mathbb{R}^{d_v}$ from the class token. Crucially, through the quantity alignment objective described later (Section 3.4), the encoder learns to implicitly encode quantity information within visual features, enabling accurate counting even when numerical supervision is unavailable at inference.

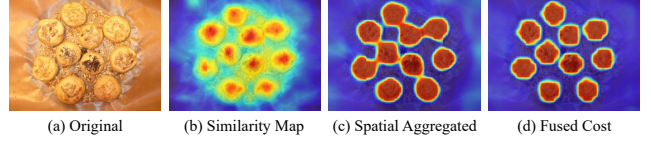


Figure 3. **Visualization of the CAD pipeline.** (a) Original image. (b) The similarity map derived from the fine-tuned CLIP exhibits **fine-grained quantity awareness**, effectively highlighting target instances while suppressing noise. (c) The aggregated cost map and (d) the final fused map demonstrate the recovery of **fine-grained spatial structure**, transforming coarse activations into precise density predictions.

3.3. Cost Aggregation Decoder

Compared to previous work [25, 28, 47], CAD operates directly on vision-text similarity maps rather than intermediate feature. This cost-based paradigm maintains the integrity of the pretrained embedding space while enabling robust fine-tuning [21]. Critically, to ensure training-inference consistency (Section 3.2), we compute similarity maps using category embeddings $\mathbf{T}_k^{\text{cat}}$ rather than $\mathbf{T}_k^{\text{full}}$.

For each quantity hypothesis k , we compute the cosine similarity between dense visual embeddings and the corresponding category embedding as

$$\mathbf{S}_k(i) = \frac{\mathbf{V}(i) \cdot \mathbf{T}_k^{\text{cat}}}{\|\mathbf{V}(i)\| \|\mathbf{T}_k^{\text{cat}}\|} \quad (4)$$

where i denotes spatial position and $\mathbf{S}_k \in \mathbb{R}^{h \times w}$ represents the similarity map. This design ensures that both training and inference compute similarities based solely on categorical matching, with quantity information implicitly encoded in visual features. We embed this similarity map into a higher-dimensional feature space through a convolutional layer, obtaining $\mathbf{G}_k \in \mathbb{R}^{h \times w \times d_g}$ where d_g is the embedding dimension.

The embedded similarity features are refined through spatial aggregation that leverages image structure to enhance localization. We employ Swin Transformer blocks for their computational efficiency and global receptive fields, operating independently on each quantity hypothesis as

$$\mathbf{G}'_k = \mathcal{A}^{\text{spa}}(\mathbf{G}_k; \mathbf{V}) \quad (5)$$

where \mathcal{A}^{spa} denotes the spatial aggregation module consisting of consecutive Swin Transformer blocks with windowed and shifted-window attention patterns. Inspired by [5, 55], we optionally provide visual embeddings \mathbf{V} as guidance to the attention computation through linear projection and concatenation to query and key features. This aggregation refines coarse similarity maps by exploiting spatial coherence, suppressing isolated activations while enhancing connected regions corresponding to actual objects.

To recover high-resolution density predictions, we progressively upsample the aggregated similarity features while incorporating multi-scale information from the vision encoder through skip connections. At each upsampling stage, we extract intermediate features from the vision encoder and modulate these connections by similarity maps to emphasize quantity-relevant regions, formulated as

$$\mathbf{G}^{(r+1)} = \text{Conv}(\text{Up}(\mathbf{G}^{(r)}) + \mathbf{W}_{\text{proj}}(\mathbf{V}_r^{\text{enc}}) \odot \sigma(\mathbf{S}_k)) \quad (6)$$

where $\mathbf{V}_r^{\text{enc}}$ denotes encoder features from stage r , \mathbf{W}_{proj} is a projection layer, and σ represents sigmoid activation. The final density map \hat{D}_k for quantity hypothesis k is obtained through a prediction head applied to the upsampled features. Figure 3 visually illustrates the entire polymerization process. For detailed illustrations of the architecture for each component, please refer to the supplementary materials.

3.4. Multi-level Quantity Alignment Loss

We introduce \mathcal{L}_{MQA} that enforces quantity awareness across multiple stages of the network through carefully designed ranking constraints. This multi-level design creates supervision signals at both encoder and decoder stages, enabling comprehensive quantity understanding throughout the pipeline.

To teach the encoder to distinguish fine-grained quantity differences, we leverage complete embeddings $\mathbf{T}_k^{\text{full}}$ that contain numerical information. We compute cosine similarities between the global image representation and all complete text embeddings as

$$\alpha_k = \frac{\mathbf{v}^g \cdot \mathbf{T}_k^{\text{full}}}{\|\mathbf{v}^g\| \|\mathbf{T}_k^{\text{full}}\|} \quad (7)$$

where α_k is the alignment score for the k -th quantity hypothesis. Let α_0 denote the similarity for the factual quantity prompt and $\{\alpha_i\}_{i=1}^{K-1}$ denote similarities for counterfactual prompts sorted by their distance from the ground truth. The encoder-level loss enforces ranking constraints as:

$$\mathcal{L}_{\text{enc}}^{\text{qty}} = \frac{1}{K-1} \sum_{i=1}^{K-1} f(\alpha_i - \alpha_0) + \frac{1}{K-3} \sum_{i=1}^{\frac{K-1}{2}-1} [f(\alpha_i - \alpha_{i+1}) + f(\alpha_{\frac{K+1}{2}+i} - \alpha_{\frac{K+1}{2}+i+1})] \quad (8)$$

where $f(\cdot)$ represents the ReLU function. The first term ensures the factual prompt achieves highest similarity, while the second enforces that prompts with counts closer to ground truth yield higher similarities. This ranking constraint teaches the encoder to implicitly encode quantity information in visual features by establishing correspondence between visual quantity prompts and numerical values in text.

At the decoder level, we enforce that predicted counts align with their corresponding quantity hypotheses, creating auxiliary supervision signals that fully utilize multiple density predictions. For each density map \hat{D}_k , we compute the predicted count $\hat{n}_k = \sum \hat{D}_k$ and enforce

$$\mathcal{L}_{\text{dec}}^{\text{qty}} = \|\hat{n}_0 - n^{\text{gt}}\|_2^2 + \beta \sum_{k=1}^{K-1} \|\hat{n}_k - q_k\|_2^2 \quad (9)$$

where q_k represents the quantity value in the k -th prompt and $\beta = 0.1$ (experientially) controls the weight of auxiliary terms. The first term ensures accurate counting for the factual hypothesis, while the auxiliary terms encourage the decoder to learn quantity-dependent prediction patterns.

The complete training objective combines density estimation loss with multi-level quantity alignment as:

$$\mathcal{L}_{\text{MQA}} = \|\hat{D}_0 - D^{\text{GT}}\|_2^2 + \lambda_1 \mathcal{L}_{\text{enc}}^{\text{qty}} + \lambda_2 \mathcal{L}_{\text{dec}}^{\text{qty}} \quad (10)$$

where \hat{D}_0 corresponds to the factual quantity prediction and $\lambda_1 = 0.1$, $\lambda_2 = 0.05$ balance the loss terms. During training, we process each image with multiple quantity-oriented text prompts, performing independent forward passes for each hypothesis while sharing encoder parameters. This creates diverse supervision signals from a single sample, enabling quantity-sensitive learning. At inference, only a category-specific prompt is provided, and the model produces density predictions by leveraging the quantity understanding implicitly acquired during training.

4. Experiments

4.1. Experimental Setup

Datasets: We conduct comprehensive experiments to validate the effectiveness of QICA on standard benchmarks for ZSOC. Primary evaluation dataset is FSC-147 [50], which comprises 6,135 images spanning 147 diverse object categories. The dataset is partitioned into 3,659 training images, 1,286 validation images, and 1,190 test images. To assess cross-domain generalization capability, we additionally evaluate on CARPK and ShanghaiTech-A [70] without any fine-tuning. The CARPK dataset contains 1,448 parking lot images captured from drone perspectives at approximately 40 meters altitude, collectively annotating nearly 90,000 vehicles. The ShanghaiTech-A dataset contains 300 train and 182 test images of dense crowd.

Implementation Details: We implement QICA with two backbone configurations: CLIP ViT-B/16 and ViT-L/14, leveraging stronger pretrained representations with minimal additional trainable parameters. Both CLIP encoders remain frozen during training, with adaptation via learnable prompts in the first 9 layers (length= 2). Text encoder uses 12 layers with dimension 512, while vision encoders vary in depth (12 vs 24 layers) and dimension (768 vs 1024). ViT-B/16

Table 1. **Performance comparison** of QICA with other SOTA models on FSC-147 dataset. The best performance for each scheme is highlighted in **bold**, and the second-best performance for the zero-shot setting is underlined.

Scheme	Method	Venue	Exemplar	Backbone	Val		Test		Avg.	
					MAE↓	RMSE↓	MAE↓	RMSE↓	MAE↓	RMSE↓
Few-shot	FamNet [50]	CVPR'21	Visual	ResNet-50	24.32	70.94	22.56	101.54	23.44	86.24
	CountTR [34]	WACV'22	Visual	ViT-B/16	13.13	49.83	11.95	91.23	12.54	70.53
	LOCA [10]	ICCV'23	Visual	ResNet-50	10.24	<u>32.56</u>	10.97	<u>56.97</u>	10.61	<u>44.77</u>
	PseCo [22]	CVPR'24	Visual	SAM-ViT-H/16	15.31	68.34	13.05	112.89	14.18	90.62
	CountGD [2]	NeurIPS'24	Visual & Text	GDINO-Swin-B	7.10	26.08	6.75	43.65	6.93	34.87
	CountSE [36]	ICCV'25	Text	GDINO-Swin-B	<u>8.51</u>	54.93	7.84	82.99	8.18	68.96
	TMR [27]	ICCV'25	Visual	SAM-ViT-H/16	-	-	11.63	57.46	11.63	57.46
Zero-shot	ZSC [62]	CVPR'23	Text	ResNet-50	26.93	88.63	22.09	115.17	24.51	101.90
	CLIP-Count [25]	ACM MM'23	Text	ViT-B/16	18.79	61.18	17.78	106.62	18.29	83.90
	CounTX [1]	BMVC'23	Text	ViT-B/16	17.76	65.21	16.70	105.21	17.23	85.21
	VA-Count [72]	ECCV'24	Text	ViT-B/16	17.87	73.22	17.88	129.31	17.88	101.27
	VLCounter [28]	AAAI'24	Text	ViT-B/16	18.06	65.13	17.05	106.16	17.56	85.65
	DAVE [43]	CVPR'24	Visual	ResNet-50	15.48	52.57	14.90	103.42	15.19	78.00
	GeCo [42]	NeurIPS'24	Visual	SAM-ViT-H/16	14.81	64.95	13.30	108.72	14.06	86.84
	CountGD [2]	NeurIPS'24	Text	GDINO-Swin-B	12.14	47.51	14.76	120.42	13.45	83.97
	T2ICount [47]	CVPR'25	Text	Stable Diff-v1.5	13.78	58.78	11.76	97.86	<u>12.77</u>	78.32
	YOLO-Count [64]	ICCV'25	Text	YOLOv8-L	14.80	96.14	15.43	58.36	15.12	<u>77.25</u>
	QICA	Ours	Text	ViT-B/16	13.82	60.24	13.05	104.17	13.44	82.21
	QICA [†]	Ours	Text	ViT-L/14	<u>12.98</u>	<u>56.35</u>	<u>12.41</u>	<u>97.28</u>	12.70	76.82

processes 384×384 images into 24×24 features, whereas ViT-L/14 handles 392×392 images producing 28×28 features. The decoder employs 2 Swin Transformer blocks (dimension 128) with two-stage upsampling and adaptive skip connections (from layers 4 and 8 for ViT-B/16, layers 8 and 16 for ViT-L/14). Training uses AdamW optimizer for 200 epochs with learning rate 1×10^{-4} and weight decay 1×10^{-2} . We generate $K = 5$ quantity hypotheses per image via adaptive interval binning, with loss weights $\lambda_1 = 0.1$ and $\lambda_2 = 0.05$. Standard augmentations are applied. Evaluation uses MAE and RMSE metrics on NVIDIA 80G A800 GPUs. Detailed information are in the Appendix.

4.2. Comparison with Advanced Methods

Results on FSC-147: We evaluate QICA against recent methods on FSC-147 in Table 1. ViT-L/14 configuration achieves 12.41 MAE and 97.28 RMSE on the test set, establishing competitive performance within the zero-shot counting paradigm. Compared to CLIP-based methods VLCounter, CLIP-Count, and CounTX, QICA demonstrates improvements of 27.2%, 30.2%, and 25.7% respectively. ViT-B/16 variant attains 13.05 MAE, surpassing CountGD despite using lighter CLIP backbone, suggesting our cost aggregation effectively preserves pretrained knowledge. Compared to diffusion-based T2ICount, QICA remains competitive with 0.65 MAE gap while exhibiting superior generalization as evidenced by minimal validation-test variance versus CountGD text mode degradation of 2.62 MAE. Both configurations substantially outperform earlier zero-shot methods, validating the effectiveness of different components.

Table 2. Comparison with SOTA methods on CARPK.

Method	Exemplar	Fine-tuned	MAE↓	RMSE↓
CountTR [34]	Visual	✓	5.75	7.45
LOCA [10]	Visual	✗	9.97	12.51
CountGD [2]	Visual & Text	✗	3.68	5.17
CLIP-Count [25]	Text	✗	11.96	16.61
CounTX [1]	Text	✓	8.13	10.87
VA-Count [72]	Text	✗	10.63	13.20
VLCounter [28]	Text	✗	6.46	8.68
CountGD [2]	Text	✗	5.98	7.41
T2ICount [47]	Text	✗	8.61	13.47
QICA (Ours)	Text	✗	6.38	8.20
QICA [†] (Ours)	Text	✗	<u>6.07</u>	<u>7.82</u>

Results on CARPK: We evaluate cross-domain generalization on CARPK without fine-tuning as shown in Table 2. QICA achieves 6.07 MAE with ViT-L/14 and 6.38 MAE with ViT-B/16, exhibiting 51% error reduction from FSC-147. While CountGD attains 3.83 MAE through specialized grounding capabilities, QICA demonstrates competitive text-based performance, surpassing T2ICount and approaching DINOv2-based methods. The consistent ViT-L/14 advantage validates our architecture scalability.

Results on ShanghaiTech-A: On ShanghaiTech-A featuring extreme crowd density, QICA establishes new SOTA among open-set methods as shown in Table 3. ViT-L/14 achieves 140.7 MAE and 258.3 RMSE, surpassing CountGD (141.9 MAE) despite using lighter CLIP features. ViT-B/16 attains 146.2 MAE, outperforming CLIP-Count and CounTX by

Table 3. Comparison with SOTA methods including specific category counting on ShanghaiTech-A test set. * means the results are reproduced by open-source codes.

Method	Category	MAE↓	RMSE↓
MCNN [70]	Specific	221.4	357.8
CrowdClip [31]	Specific	217.0	322.7
RCC [19]	Open-set	240.1	366.9
CounTX [1]	Open-set	219.8	351.0
CLIP-Count [25]	Open-set	192.6	308.4
CountGD* [2]	Open-set	<u>141.9</u>	258.0
VLP [65]	Open-set	178.9	284.6
QICA	Open-set	146.2	269.6
QICA [†]	Open-set	140.7	<u>258.3</u>

Table 4. Ablation Study on FSC-147. ‘TP’ refers ‘Text Prompts only’ (no quantity), ‘SP’ represents ‘Synergistic Prompting’. Baseline/intermediate configurations (rows 1-3) process \mathbf{V} directly, while CAD configurations (rows 4-5) operate on $\mathbf{V-T}^{cat}$ similarity maps.

TP	SP	CAD	\mathcal{L}_{MQA}	Val		Test	
				MAE↓	RMSE↓	MAE↓	RMSE↓
○	○	○	○	16.82	68.45	16.15	124.32
●	○	○	○	15.46	63.28	14.89	115.63
○	●	○	○	14.27	59.14	13.72	107.85
○	●	●	○	13.41	57.62	12.88	99.74
○	●	●	●	12.98	56.35	12.41	97.28

24.1% and 33.5% respectively. This validates that our cost aggregation and quantity-aware prompting effectively address dense localization challenges, with spatial aggregation proving particularly valuable in extreme counting scenarios.

4.3. Ablation Study

We systematically evaluate each component contribution on FSC-147 with ViT-L/14 as shown in Table 4. From baseline CLIP fine-tuning (16.15 test MAE), adding text prompts (no quantity) reduces error to 14.89 MAE through learnable textual representations. Synergistic prompting yields 13.72 MAE with 8.0% improvement validating cross-modal adaptation effectiveness. Cost aggregation decoder achieves 12.88 MAE (6.1% gain) by preserving pretrained knowledge through similarity map operations. Multi-level quantity alignment reaches 12.41 MAE via joint encoder-decoder supervision. The cumulative 23.2% improvement confirms all components work synergistically.

5. Model Analysis

5.1. Analysis of Prompt

Prompt Depth: Figure 4a shows prompt depth effects on FSC-147 validation set. Vision-only prompting improves

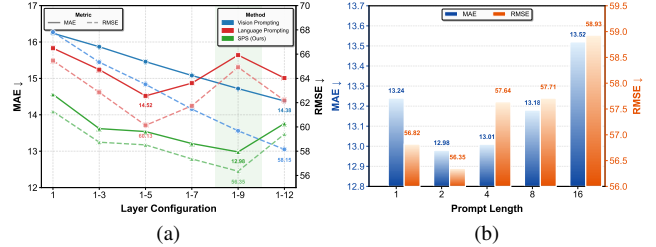


Figure 4. Ablation on prompt depth (a) and prompt length (b) in QICA. We report results on the validation sets of FSC-147.

monotonically to 14.38 MAE at 1-12 layers, while language-only peaks at 1-5 layers (14.52 MAE) before degrading. SPS achieves 12.98 MAE at 1-9 layers, outperforming both unimodal strategies by enabling complementary adaptation where quantity-aware text guides vision refinement.

Prompt Length: Figure 4b illustrates length sensitivity. Optimal performance occurs at length 2 (12.98 MAE), with degradation beyond length 4. This indicates compact prompts sufficiently encode quantity semantics while avoiding over-parameterization, contrasting with assumptions that longer prompts provide greater expressiveness.

Table 5. Results for different value of K on FSC-147. More results are in the appendix.

	K	1	3	5	7
Val	MAE↓	13.76	13.21	12.98	13.12
	RMSE↓	58.24	57.16	56.35	56.89
Test	MAE↓	13.18	12.67	12.41	12.58
	RMSE↓	101.45	98.92	97.28	98.16

Number of Quantity K: Table 5 examines \mathbf{K} effects on FSC-147. Using only factual hypothesis ($\mathbf{K}=1$) yields 13.76 validation MAE, while $\mathbf{K}=5$ achieves optimal performance at 12.98 validation MAE and 12.41 test MAE through symmetric counterfactual pairs. Further increasing to $\mathbf{K}=7$ degrades performance to 13.12 MAE, indicating excessive hypotheses introduce optimization challenges without benefits.

5.2. Effect of Loss Weight

Figure 5 presents sensitivity analysis of loss weights λ_1 and λ_2 on FSC-147 validation set. For decoder quantity consistency, $\lambda_1 = 0.1$ achieves optimal 12.98 MAE, with deviations degrading performance up to 2.0%. Encoder quantity alignment exhibits higher sensitivity, where $\lambda_2 = 0.05$ reaches optimum while excessive values (0.15) degrade by 3.4%. This reflects that ranking constraints on frozen encoder outputs require careful calibration. Notably, insufficient encoder supervision ($\lambda_2 = 0.01$, 2.8% degradation) impacts performance more than insufficient decoder supervision, confirming that quantity-aware feature learning at the encoder stage is critical for effective density prediction.

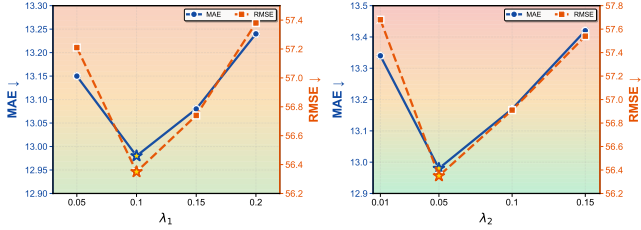


Figure 5. Sensitivity analysis of loss weights on FSC-147 validation set. Left shows the effect of λ_1 on \mathcal{L}_{enc}^{qty} while right illustrates λ_2 on \mathcal{L}_{dec}^{qty} . ★ Gold stars mark optimal configurations.

5.3. Visualization

Figure 6 compares QICA with VLCounter [28] and T2ICount [47] across diverse categories. On tree logs with irregular shapes, QICA produces smooth and spatially coherent density predictions, while VLCounter shows fragmented responses and T2ICount exhibits less precise localization. For strawberries featuring similar appearance and clustered arrangement, QICA and T2ICount achieve accurate counts near GT, whereas VLCounter overestimates due to response leakage. On sticky notes with high density and color variation, QICA approaches GT, outperforming VLCounter which severely undercounts. The visualization demonstrates that QICA’s cost aggregation decoder produces more refined spatial distributions with better boundary delineation, validating its effectiveness in preserving quantity-aware localization across challenging scenarios.

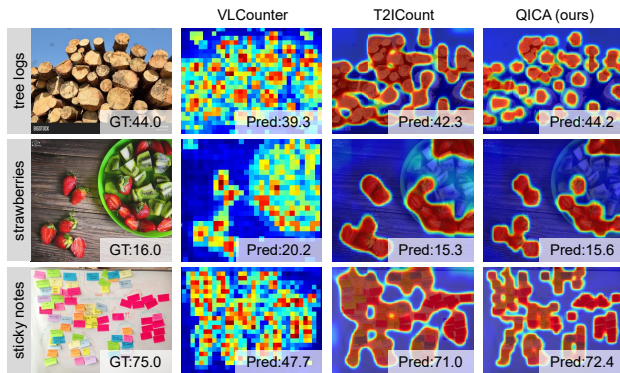


Figure 6. Qualitative comparison of QICA with VLCounter [28] and T2ICount [47]. Our text-image ‘similarity map’ exhibits reduced noise and more precise object delineation, which results in a more accurate density estimation.

5.4. Efficiency Analysis

Figure 7 presents comprehensive efficiency comparison on NVIDIA A800 GPU. QICA demonstrates exceptional parameter efficiency with only 18.5M/19.7M trainable parameters versus 25M-170M for existing methods, achieved through frozen encoders with learnable prompt adaptation. QICA-B/16 delivers 20.8G MACs and 45.2 FPS while achieving

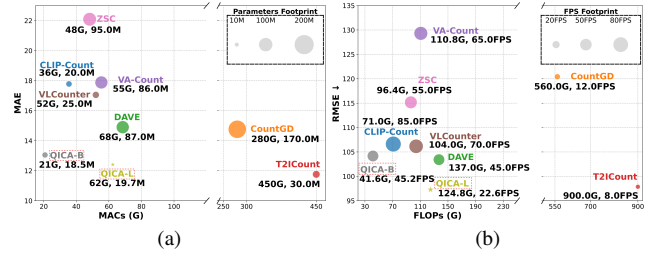


Figure 7. Efficiency analysis of QICA compared to SOTA methods. (a) Relationship between trainable parameters, MAE performance, and computational cost represented. (b) Comprehensive efficiency metrics including FLOPs and inference speed (FPS). ★ represents QICA-L (ViT-L/14) while ● is QICA-B (ViT-B/16).

superior accuracy compared to VLCounter. The ViT-L/14 variant balances computational cost with enhanced performance and competitive speed. Both configurations significantly outperform heavyweight approaches like CountGD and T2ICount, positioning QICA in the optimal efficiency-performance region for practical deployment. More detailed information are in Appendix.

6. Conclusion

We present QICA, a novel framework for ZSOC that addresses critical limitations regarding fine-grained quantity awareness and spatial insensitivity in existing approaches. Our SPS enables effective joint adaptation through explicit numerical conditioning, instilling the model with precise quantity perception via bidirectional gradient coupling. Simultaneously, the CAD overcomes spatial insensitivity by refining similarity maps. This design effectively prevents feature space distortion during adaptation while recovering the fine-grained spatial structure necessary for precise counting. Additionally, the (\mathcal{L}_{MQA}) enforces numerical consistency across encoder and decoder stages through ranking constraints. Extensive experiments demonstrate competitive performance on FSC-147, with cross-dataset evaluation on CARPK and ShanghaiTech-A validating strong zero-shot generalization to unseen domains.

Limitation and Future Work: QICA relies on discrete quantity hypotheses and focuses on single-category counting, which limits its applicability to continuous quantity relationships and multi-category scenarios. We will explore continuous quantity representations and simultaneous multi-category counting to broaden practical utility in the future.

Acknowledgements

This work was supported in part by grants from the National Natural Science Foundation of China (62576284 & 62306241), and in part by grants from the Innovation Foundation for Doctor Dissertation of Northwestern Polytechnical University (No.CX2025109).

References

- [1] Niki Amini-Naieni, Kiana Amini-Naieni, Tengda Han, and Andrew Zisserman. Open-world text-specified object counting. *arXiv preprint arXiv:2306.01851*, 2023. 6, 7
- [2] Niki Amini-Naieni, Tengda Han, and Andrew Zisserman. Countgd: Multi-modal open-world counting. *Advances in Neural Information Processing Systems*, 37:48810–48837, 2024. 1, 3, 6, 7
- [3] Lital Binyamin, Yoad Tewel, Hilit Segev, Eran Hirsch, Royi Rassin, and Gal Chechik. Make it count: Text-to-image generation with an accurate number of objects. In *Proceedings of the Computer Vision and Pattern Recognition Conference*, pages 13242–13251, 2025. 1
- [4] Zhi-Qi Cheng, Qi Dai, Hong Li, Jingkuan Song, Xiao Wu, and Alexander G Hauptmann. Rethinking spatial invariance of convolutional networks for object counting. In *Proceedings of the IEEE/CVF conference on computer vision and pattern recognition*, pages 19638–19648, 2022. 2
- [5] Seokju Cho, Heeseong Shin, Sunghwan Hong, Anurag Arnab, Paul Hongsuck Seo, and Seungryong Kim. Cat-seg: Cost aggregation for open-vocabulary semantic segmentation. In *Proceedings of the IEEE/CVF Conference on Computer Vision and Pattern Recognition*, pages 4113–4123, 2024. 4
- [6] Siyang Dai, Jun Liu, and Ngai-Man Cheung. Referring expression counting. In *Proceedings of the IEEE/CVF Conference on Computer Vision and Pattern Recognition*, pages 16985–16995, 2024. 1
- [7] Stefano Damiano, Luca Bondi, Shabnam Ghaffarzagdegan, Andre Guntoro, and Toon Van Waterschoot. Can synthetic data boost the training of deep acoustic vehicle counting networks? In *ICASSP 2024-2024 IEEE International Conference on Acoustics, Speech and Signal Processing (ICASSP)*, pages 631–635. IEEE, 2024. 2
- [8] Perla Doubinsky, Nicolas Audebert, Michel Crucianu, and Hervé Le Borgne. Semantic generative augmentations for few-shot counting. In *Proceedings of the IEEE/CVF Winter Conference on Applications of Computer Vision*, pages 5443–5452, 2024. 3
- [9] Yao Du, Qiang Zhai, Weihang Dai, and Xiaomeng Li. Teach clip to develop a number sense for ordinal regression. In *European Conference on Computer Vision*, pages 1–17. Springer, 2024. 2, 3
- [10] Nikola Dukić, Alan Lukežič, Vitjan Zavrtanik, and Matej Kristan. A low-shot object counting network with iterative prototype adaptation. In *Proceedings of the IEEE/CVF International Conference on Computer Vision (ICCV)*, pages 18872–18881, 2023. 2, 6
- [11] Qi Fan, Wei Zhuo, Chi-Keung Tang, and Yu-Wing Tai. Few-shot object detection with attention-rpn and multi-relation detector. In *Proceedings of the IEEE/CVF conference on computer vision and pattern recognition*, pages 4013–4022, 2020. 2
- [12] Stephanie Fu, Tyler Bonnen, Devin Guillory, and Trevor Darrell. Hidden in plain sight: VLMs overlook their visual representations. *arXiv preprint arXiv:2506.08008*, 2025. 2
- [13] Guangshuai Gao, Junyu Gao, Qingjie Liu, Qi Wang, and Yunhong Wang. A survey of deep learning methods for density estimation and crowd counting. *Vicinagearth*, 2(1):1–37, 2025. 1
- [14] Junyu Gao, Tao Han, Yuan Yuan, and Qi Wang. Domain-adaptive crowd counting via high-quality image translation and density reconstruction. *IEEE transactions on neural networks and learning systems*, 34(8):4803–4815, 2021. 2
- [15] Junyu Gao, Da Zhang, Feiyu Wang, Lichen Ning, Zhiyuan Zhao, and Xuelong Li. Combining sam with limited data for change detection in remote sensing. *IEEE Transactions on Geoscience and Remote Sensing*, 2025. 2
- [16] Junyu Gao, Da Zhang, Qiyu Wang, Zhiyuan Zhao, and Xuelong Li. Dynamic proxy domain generalizes the crowd localization by better binary segmentation. *Pattern Recognition*, page 112481, 2025. 1
- [17] Xuyang Guo, Zekai Huang, Zhenmei Shi, Zhao Song, and Jiahao Zhang. Your vision-language model can’t even count to 20: Exposing the failures of vlms in compositional counting. *arXiv preprint arXiv:2510.04401*, 2025. 2, 3
- [18] Ian A Hatton, Eric D Galbraith, Nono SC Merleau, Teemu P Miettinen, Benjamin McDonald Smith, and Jeffery A Shander. The human cell count and size distribution. *Proceedings of the National Academy of Sciences*, 120(39):e2303077120, 2023. 2
- [19] Michael Hobley and Victor Prisacariu. Learning to count anything: Reference-less class-agnostic counting with weak supervision. *arXiv preprint arXiv:2205.10203*, 2022. 7
- [20] Meng-Ru Hsieh, Yen-Liang Lin, and Winston H Hsu. Drone-based object counting by spatially regularized regional proposal network. In *Proceedings of the IEEE international conference on computer vision*, pages 4145–4153, 2017. 2
- [21] Edward J Hu, Yelong Shen, Phillip Wallis, Zeyuan Allen-Zhu, Yuanzhi Li, Shean Wang, Lu Wang, Weizhu Chen, et al. Lora: Low-rank adaptation of large language models. *ICLR*, 1(2):3, 2022. 4
- [22] Zhizhong Huang, Mingliang Dai, Yi Zhang, Junping Zhang, and Hongming Shan. Point segment and count: A generalized framework for object counting. In *Proceedings of the IEEE/CVF Conference on Computer Vision and Pattern Recognition*, pages 17067–17076, 2024. 1, 6
- [23] Xiaofei Hui, Qian Wu, Hossein Rahmani, and Jun Liu. Class-agnostic object counting with text-to-image diffusion model. In *European Conference on Computer Vision*, pages 1–18. Springer, 2024. 1
- [24] Menglin Jia, Luming Tang, Bor-Chun Chen, Claire Cardie, Serge Belongie, Bharath Hariharan, and Ser-Nam Lim. Visual prompt tuning. In *European conference on computer vision*, pages 709–727. Springer, 2022. 2
- [25] Ruixiang Jiang, Lingbo Liu, and Changwen Chen. Clipcount: Towards text-guided zero-shot object counting. In *Proceedings of the 31st ACM International Conference on Multimedia*, pages 4535–4545, 2023. 3, 4, 6, 7
- [26] Xiaolong Jiang, Zehao Xiao, Baochang Zhang, Xiantong Zhen, Xianbin Cao, David Doermann, and Ling Shao. Crowd counting and density estimation by trellis encoder-decoder networks. In *Proceedings of the IEEE/CVF conference on computer vision and pattern recognition*, pages 6133–6142, 2019. 2

- [27] Eunchan Jo, Dahyun Kang, Sanghyun Kim, Yunseon Choi, and Minsu Cho. Few-shot pattern detection via template matching and regression. In *Proceedings of the IEEE/CVF International Conference on Computer Vision*, pages 21578–21588, 2025. 6
- [28] Seunggu Kang, WonJun Moon, Euiyeon Kim, and Jae-Pil Heo. Vlcounter: Text-aware visual representation for zero-shot object counting. In *Proceedings of the AAAI Conference on Artificial Intelligence*, pages 2714–2722, 2024. 1, 3, 4, 6, 8
- [29] Muhammad Uzair Khattak, Hanoona Rasheed, Muhammad Maaz, Salman Khan, and Fahad Shahbaz Khan. Maple: Multi-modal prompt learning. In *Proceedings of the IEEE/CVF conference on computer vision and pattern recognition*, pages 19113–19122, 2023. 2, 3
- [30] Ming Li, Yupeng Hu, Yinwei Wei, Hao Liu, Haocong Wang, and Weili Guan. Dcount: Decoupled spatial perception and attribute discrimination for referring expression counting. In *Proceedings of the 33rd ACM International Conference on Multimedia*, pages 5306–5315, 2025. 2
- [31] Dingkan Liang, Jiahao Xie, Zhikang Zou, Xiaoqing Ye, Wei Xu, and Xiang Bai. Crowdclip: Unsupervised crowd counting via vision-language model. In *Proceedings of the IEEE/CVF conference on computer vision and pattern recognition*, pages 2893–2903, 2023. 1, 2, 7
- [32] Wei Lin and Antoni B Chan. A fixed-point approach to unified prompt-based counting. In *Proceedings of the AAAI Conference on Artificial Intelligence*, pages 3468–3476, 2024. 1, 2
- [33] Wei Lin, Chenyang Zhao, and Antoni B Chan. Point-to-region loss for semi-supervised point-based crowd counting. In *Proceedings of the Computer Vision and Pattern Recognition Conference*, pages 29363–29373, 2025. 1
- [34] Chang Liu, Yujie Zhong, Andrew Zisserman, and Weidi Xie. Countr: Transformer-based generalised visual counting. *arXiv preprint arXiv:2208.13721*, 2022. 2, 6
- [35] Chengxin Liu, Hao Lu, Zhiguo Cao, and Tongliang Liu. Point-query quadtree for crowd counting, localization, and more. In *Proceedings of the IEEE/CVF international conference on computer vision*, pages 1676–1685, 2023. 2
- [36] Shuai Liu, Peng Zhang, Shiwei Zhang, and Wei Ke. Countse: Soft exemplar open-set object counting. In *Proceedings of the IEEE/CVF International Conference on Computer Vision*, pages 21536–21546, 2025. 2, 3, 6
- [37] Erika Lu, Weidi Xie, and Andrew Zisserman. Class-agnostic counting. In *Asian conference on computer vision*, pages 669–684. Springer, 2018. 1, 2
- [38] Rui Ma, Yi Hou, Chenxuan Li, Huizhu Jia, and Xiaodong Xie. Scene-adaptive unsupervised crowd counting for video surveillance. *IEEE Transactions on Circuits and Systems for Video Technology*, 2025. 1, 2
- [39] Anindya Mondal, Sauradip Nag, Xiatian Zhu, and Anjan Dutta. Omnicount: Multi-label object counting with semantic-geometric priors. In *Proceedings of the AAAI Conference on Artificial Intelligence*, pages 19537–19545, 2025. 1
- [40] Trong Bang Nguyen, Phi Le Nguyen, Simon Lucey, and Minh Hoai. Region-level data attribution for text-to-image generative models. In *Proceedings of the IEEE/CVF International Conference on Computer Vision*, pages 18825–18833, 2025. 2
- [41] Roni Paiss, Ariel Ephrat, Omer Tov, Shiran Zada, Inbar Mosseri, Michal Irani, and Tali Dekel. Teaching clip to count to ten. In *Proceedings of the IEEE/CVF International Conference on Computer Vision*, pages 3170–3180, 2023. 2, 3
- [42] Jer Pelhan, Alan Lukezic, Vitjan Zavrtanik, and Matej Kristan. A novel unified architecture for low-shot counting by detection and segmentation. *Advances in Neural Information Processing Systems*, 37:66260–66282, 2024. 6
- [43] Jer Pelhan, Vitjan Zavrtanik, Matej Kristan, et al. Dave-a detect-and-verify paradigm for low-shot counting. In *Proceedings of the IEEE/CVF Conference on Computer Vision and Pattern Recognition*, pages 23293–23302, 2024. 1, 3, 6
- [44] Wujian Peng, Sicheng Xie, Zuyao You, Shiyi Lan, and Zuxuan Wu. Synthesize diagnose and optimize: Towards fine-grained vision-language understanding. In *Proceedings of the IEEE/CVF Conference on Computer Vision and Pattern Recognition*, pages 13279–13288, 2024. 2
- [45] Ahmed Qazi, Taha Razzaq, and Asim Iqbal. Animalformer: Multimodal vision framework for behavior-based precision livestock farming. In *Proceedings of the IEEE/CVF Conference on Computer Vision and Pattern Recognition*, pages 7973–7982, 2024. 1
- [46] Muhammad Fetrat Qharabagh, Mohammadreza Ghofrani, and Kimon Fountoulakis. Lvlm-count: Enhancing the counting ability of large vision-language models. *arXiv preprint arXiv:2412.00686*, 2024. 2
- [47] Yifei Qian, Zhongliang Guo, Bowen Deng, Chun Tong Lei, Shuai Zhao, Chun Pong Lau, Xiaopeng Hong, and Michael P Pound. T2icount: Enhancing cross-modal understanding for zero-shot counting. In *Proceedings of the Computer Vision and Pattern Recognition Conference*, pages 25336–25345, 2025. 1, 3, 4, 6, 8
- [48] Alec Radford, Jong Wook Kim, Chris Hallacy, Aditya Ramesh, Gabriel Goh, Sandhini Agarwal, Girish Sastry, Amanda Askell, Pamela Mishkin, Jack Clark, et al. Learning transferable visual models from natural language supervision. In *International conference on machine learning*, pages 8748–8763. PmLR, 2021. 2
- [49] Viresh Ranjan and Minh Hoai Nguyen. Exemplar free class agnostic counting. In *Proceedings of the Asian Conference on Computer Vision*, pages 3121–3137, 2022. 1, 2
- [50] Viresh Ranjan, Udbhav Sharma, Thu Nguyen, and Minh Hoai. Learning to count everything. In *Proceedings of the IEEE/CVF Conference on Computer Vision and Pattern Recognition*, pages 3394–3403, 2021. 2, 5, 6
- [51] Chenggang Rong, Tao Han, Zhiyuan Zhao, Yaowu Fan, Jia Wan, Song Guo, Yuan Yuan, and Junyu Gao. Unicbench: Unified counting benchmark for mllm. *arXiv preprint arXiv:2603.00595*, 2026. 2
- [52] Min Shi, Hao Lu, Chen Feng, Chengxin Liu, and Zhiguo Cao. Represent, compare, and learn: A similarity-aware framework for class-agnostic counting. In *Proceedings of the IEEE/CVF Conference on Computer Vision and Pattern Recognition*, pages 9529–9538, 2022. 2
- [53] Miaoqing Shi, Xiaowen Zhang, Zijie Yue, Yong Luo, Cairong Zhao, and Li Li. Text-promptable object counting via quantity

- awareness enhancement. *arXiv preprint arXiv:2507.06679*, 2025. 2
- [54] Weibo Shu, Jia Wan, Kay Chen Tan, Sam Kwong, and Antoni B Chan. Crowd counting in the frequency domain. In *Proceedings of the IEEE/CVF conference on computer vision and pattern recognition*, pages 19618–19627, 2022. 2
- [55] Deqing Sun, Xiaodong Yang, Ming-Yu Liu, and Jan Kautz. Pwc-net: Cnns for optical flow using pyramid, warping, and cost volume. In *Proceedings of the IEEE conference on computer vision and pattern recognition*, pages 8934–8943, 2018. 4
- [56] Mingjie Wang, Song Yuan, Zhuohang Li, Longlong Zhu, Eric Buys, and Minglun Gong. Language-guided zero-shot object counting. In *2024 IEEE International Conference on Multimedia and Expo Workshops (ICMEW)*, pages 1–6. IEEE, 2024. 1
- [57] Mingjie Wang, Jun Zhou, Yong Dai, Eric Buys, and Minglun Gong. Enhancing zero-shot counting via language-guided exemplar learning. *arXiv preprint arXiv:2402.05394*, 2024. 3
- [58] Qi Wang, Junyu Gao, Wei Lin, and Xuelong Li. Nwpu-crowd: A large-scale benchmark for crowd counting and localization. *IEEE transactions on pattern analysis and machine intelligence*, 43(6):2141–2149, 2020. 1, 2
- [59] Zhicheng Wang, Zhiyu Pan, Zhan Peng, Jian Cheng, Liwen Xiao, Wei Jiang, and Zhiguo Cao. Exploring contextual attribute density in referring expression counting. In *Proceedings of the Computer Vision and Pattern Recognition Conference*, pages 19587–19596, 2025. 1
- [60] Mitchell Wortsman, Gabriel Ilharco, Jong Wook Kim, Mike Li, Simon Kornblith, Rebecca Roelofs, Raphael Gontijo Lopes, Hannaneh Hajishirzi, Ali Farhadi, Hongseok Namkoong, et al. Robust fine-tuning of zero-shot models. In *Proceedings of the IEEE/CVF conference on computer vision and pattern recognition*, pages 7959–7971, 2022. 2
- [61] Weidi Xie, J Alison Noble, and Andrew Zisserman. Microscopy cell counting and detection with fully convolutional regression networks. *Computer methods in biomechanics and biomedical engineering: Imaging & Visualization*, 6(3): 283–292, 2018. 2
- [62] Jingyi Xu, Hieu Le, Vu Nguyen, Viresh Ranjan, and Dimitris Samaras. Zero-shot object counting. In *Proceedings of the IEEE/CVF Conference on Computer Vision and Pattern Recognition*, pages 15548–15557, 2023. 1, 2, 6
- [63] Shuo-Diao Yang, Hung-Ting Su, Winston H Hsu, and Wen-Chin Chen. Class-agnostic few-shot object counting. In *Proceedings of the IEEE/CVF Winter Conference on Applications of Computer Vision*, pages 870–878, 2021. 2
- [64] Guanning Zeng, Xiang Zhang, Zirui Wang, Haiyang Xu, Zeyuan Chen, Bingnan Li, and Zhuowen Tu. Yolo-count: Differentiable object counting for text-to-image generation. In *Proceedings of the IEEE/CVF International Conference on Computer Vision*, pages 16765–16775, 2025. 2, 6
- [65] Wenzhe Zhai, Xianglei Xing, Mingliang Gao, and Qilei Li. Zero-shot object counting with vision-language prior guidance network. *IEEE Transactions on Circuits and Systems for Video Technology*, 2024. 7
- [66] Da Zhang, Feiyu Wang, Lichen Ning, Zhiyuan Zhao, Junyu Gao, and Xuelong Li. Integrating sam with feature interaction for remote sensing change detection. *IEEE Transactions on Geoscience and Remote Sensing*, 62:1–11, 2024. 1
- [67] Da Zhang, Feiyu Wang, Bingyu Li, Zhiyuan Zhao, Junyu Gao, and Xuelong Li. Kaid: Knowledge-aware interactive distillation for vision-language models. In *Proceedings of the 33rd ACM International Conference on Multimedia*, pages 3212–3221, 2025. 1
- [68] Da Zhang, Bingyu Li, Feiyu Wang, Zhiyuan Zhao, Junyu Gao, and Xuelong Li. Cross-attention multi-scale state space model for remaining useful life prediction of aircraft engines. *Advanced Engineering Informatics*, 69:103817, 2026. 1
- [69] Shiwei Zhang, Qi Zhou, and Wei Ke. Enhancing zero-shot object counting via text-guided local ranking and number-evoked global attention. In *Proceedings of the IEEE/CVF International Conference on Computer Vision*, pages 21097–21106, 2025. 2, 3
- [70] Yingying Zhang, Desen Zhou, Siqin Chen, Shenghua Gao, and Yi Ma. Single-image crowd counting via multi-column convolutional neural network. In *Proceedings of the IEEE conference on computer vision and pattern recognition*, pages 589–597, 2016. 5, 7
- [71] Kaiyang Zhou, Jingkang Yang, Chen Change Loy, and Ziwei Liu. Learning to prompt for vision-language models. *International Journal of Computer Vision*, 130(9):2337–2348, 2022. 2, 3
- [72] Huilin Zhu, Jingling Yuan, Zhengwei Yang, Yu Guo, Zheng Wang, Xian Zhong, and Shengfeng He. Zero-shot object counting with good exemplars. In *European Conference on Computer Vision*, pages 368–385. Springer, 2024. 3, 6